Journal of Alloys and Compounds 835 (2020) 155320

Contents lists available at ScienceDirect

Journal of Alloys and Compounds

journal homepage: http://www.elsevier.com/locate/jalcom

(1-*x*)Li_4WO_5-*x*LiF: A novel oxyfluoride system and their microwave dielectric properties

Kai Xiao [a, 1], Chunchun Li [a, 1], Ying Tang [a, **], Yunfei Tian [a], Changzhi Yin [a], Junqi Chen [a], Jie Li [a], Lian Duan [a], Huaicheng Xiang [a], Liang Fang [a, b, *]

[a] Guangxi Key Laboratory of Optical and Electronic Materials and Devices, Collaborative Innovation Center for Exploration of Hidden Nonferrous Metal Deposits and Development of New Materials in Guangxi, College of Material Science and Engineering, Guilin University of Technology, Guilin, 541004, China
[b] College of Materials and Chemical Engineering, China Three Gorges University, Yichang, 443002, China

ARTICLE INFO

Article history:
Received 9 December 2019
Received in revised form
21 April 2020
Accepted 21 April 2020
Available online 28 April 2020

Keywords:
Degree of order
Relative density
Microwave dielectric properties
Rock salt structure

ABSTRACT

A series of novel oxyfluorides in the (1-*x*)Li_4WO_5-*x*LiF (x = 0.1, 0.2, 0.3, 0.4, 0.5) binary system were prepared by the conventional solid-state ceramic route and their microwave dielectric properties were reported. Phase transformation form cubic to triclinic was confirmed via XRD, DTA and Raman spectra characterization. The temperature of phase transition (cubic-triclinic phase) moved towards high temperature with the increase of LiF content. EDS analysis and element mapping implied the homogenous distribution of F^- ions. Particularly, when x was equal to 0.3 (The chemical formula was $Li_{3.1}W_{0.7}F_{0.3}O_{3.5}$), the microstructure of Li_4WO_5 was evidently improved and a dense microstructure with high relative density (96.4%) was achieved. The comprehensive microwave dielectric performance of $Li_{3.1}W_{0.7}F_{0.3}O_{3.5}$ ceramics sintered at 930 °C was optimum: $Q \times f$ = 71,000 GHz, ε_r = 16.6 and τ_f = −16.4 ppm/°C. The infrared reflectivity spectra revealed that the intrinsic quality factor of $Li_{3.1}W_{0.7}F_{0.3}O_{3.5}$ ceramics was 83,000 GHz.

1. Introduction

Recently, the dielectric properties of Li-containing rock salt compounds have received considerable attention because of their ultralow dielectric loss at microwave frequency region [1–8]. Unfortunately, the sintering temperature (>960 °C) of most rock salt compounds is too high to be directly used in low-temperature cofired ceramic technology (LTCC), such as Li_2MnO_3 and Li_2MgTiO_4. So it is necessary to add sintering aids to decrease the sintering temperature [1,3]. The addition of sintering aids not only reduces the performance and complicate process, but also increases the possibility of reacting with the electrode [9–11]. Among them, Li_4WO_5 with the sintering temperature of 890 °C was reported to be a low-firing ceramic with promising microwave dielectric properties [8]. However, it is still a challenge to obtain well-sintered Li_4WO_5 ceramics with high density and low porosity for optimizing the dielectric properties, which relates to the phase transition and the Li volatilization during the high-temperature sintering process. In our previous work, non-stoichiometry with addition of extra Li were carried out in Li_4WO_5 to suppress Li volatilization, which not only improved the densification of Li_4WO_5 but also enhanced the dielectric performances [12,13]. It is concluded that lowering the sintering temperature is crucial to reduce the possibility of chemical elements volatilization. To date, the influence of phase transition on microstructural characteristics and macroscopic physical properties has not yet been reported.

Addition of sintering aids (B_2O_3, MnO_2 and LiF) with low melting points is a promising and effective approach to lower the sintering temperatures of ceramics [14–16]. Herein, LiF was selected as sintering aid for Li_4WO_5 due to its low melting point (848 °C) and successful reduction of sintering temperatures of some materials, such as Li_2TiO_3, Li_3NbO_4 [17,18]. In addition, LiF adopts the same rock salt structure with Li_4WO_5, making it possible to form solid solution. Castellanos et al. reported that Li_2TiO_3 could form solid solutions with MgO and the phase transition temperature from

* Corresponding author. Guangxi Key Laboratory of Optical and Electronic Materials and Devices, Collaborative Innovation Center for Exploration of Hidden Nonferrous Metal Deposits and Development of New Materials in Guangxi, College of Material Science and Engineering, Guilin University of Technology, Guilin, 541004, China.
** Corresponding author.
E-mail addresses: tangyinggl001@aliyun.com (Y. Tang), fanglianggl001@aliyun.com (L. Fang).
[1] Kai Xiao and Chunchun Li contributed equally to this work.

https://doi.org/10.1016/j.jallcom.2020.155320
0925-8388/

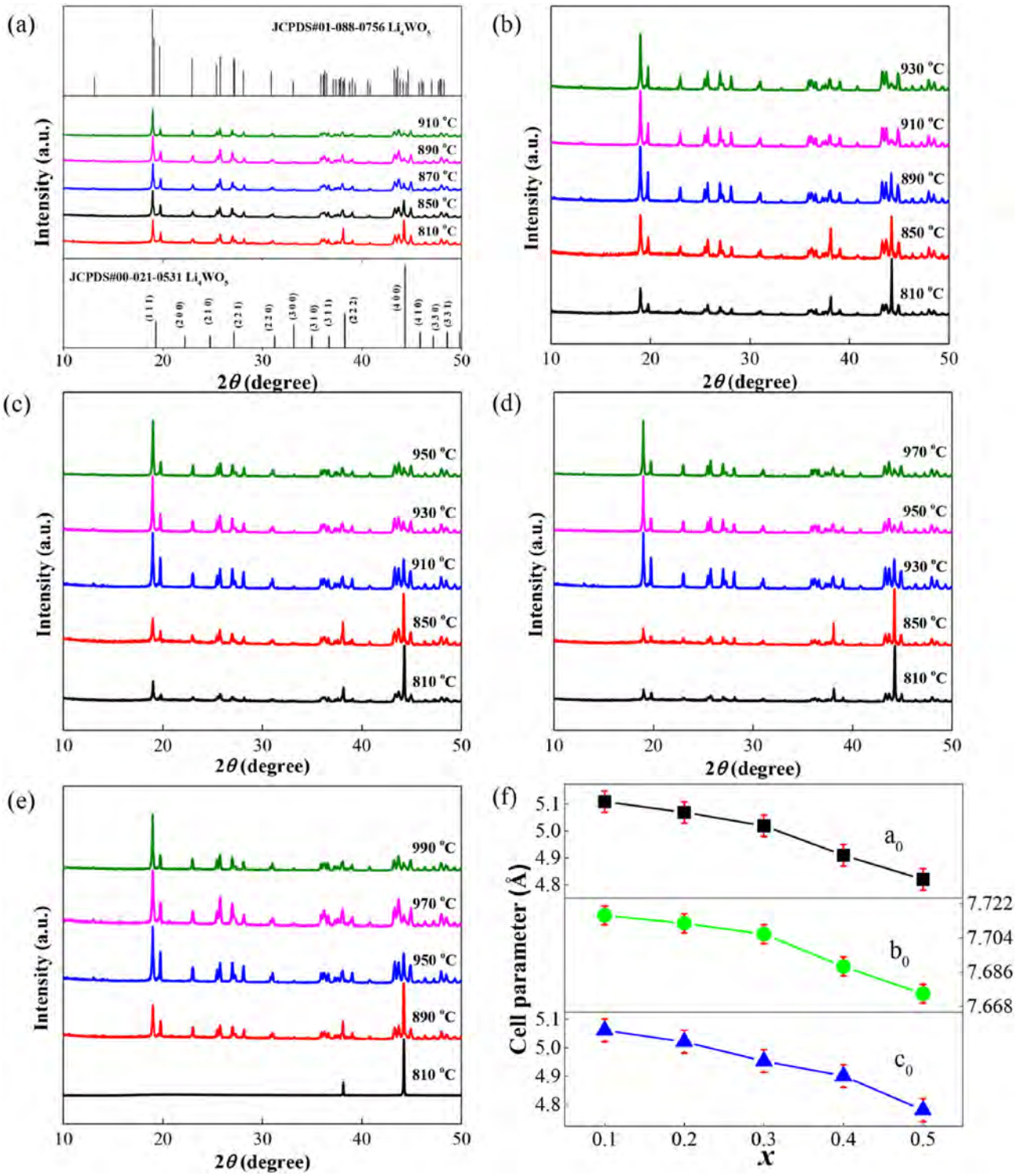

Fig. 1. (a–e) The room-temperature XRD patterns of the (1-*x*)Li_4WO_5-*x*LiF ((a) $x = 0.1$, (b) $x = 0.2$, (c) $x = 0.3$, (d) $x = 0.4$, (e) $x = 0.5$) ceramics sintered from 810 °C to 990 °C for 4 h; Fig. 1(f) the cell parameters of the triclinic phase as a function of LiF content sintered at optimum temperature.

monoclinic to cubic increased rapidly with the increase of MgO content [19]. Similarly, Li_4WO_5 might form solid solution with LiF and the phase transition temperature from cubic to triclinic might be changed. If the addition of LiF could decrease the degree of order and the sintering temperature of Li_4WO_5, the cubic phase solid solutions might be obtained. Therefore, new oxyfluorides in rock salt family are expected to obtain. In this work, a series of oxyfluorides in the (1-*x*)Li_4WO_5-*x*LiF ($x = 0.1, 0.2, 0.3, 0.4, 0.5$) binary system were prepared. The phase evolution, sintering behavior, and microwave dielectric properties were studied in detail.

2. Experimental

The starting materials of Li_2CO_3 (99.99%), WO_3(99%) were used according to the stoichiometric formula Li_4WO_5. The raw materials were ball milled for 6 h with ethanol in a nylon jar, followed by a

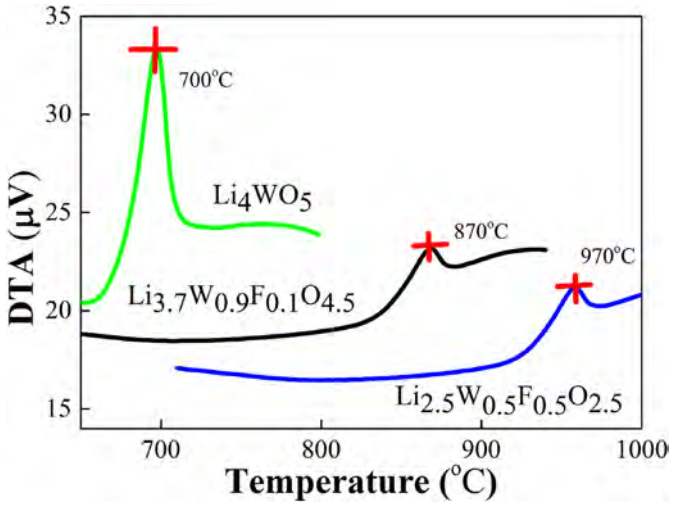

Fig. 2. DTA curves for Li_4WO_5, $Li_{3.7}W_{0.9}F_{0.1}O_{4.5}$ and $Li_{2.5}W_{0.5}F_{0.5}O_{2.5}$ powders.

treatment of drying and calcination at 600 °C for 4 h. Powders of (1-*x*)Li_4WO_5-*x*LiF (x = 0.1, 0.2, 0.3, 0.4, 0.5) were ball milled in alcohol for 6 h, then, dried and the obtained powders were mixed with 5 wt % of polyvinyl alcohol (PVA) as a binder and granulated. The resultant powders were pressed into the disks with 12 mm diameter and 6 mm thickness at 200 MPa. Pellets were sintered in air at temperature ranges from 800 °C to 1100 °C at a heating rate of 5 °C/min.

The crystal structure and phase purity of the sintered samples were identified using X-ray diffraction with CuK_α radiation (XRD; Model X'Pert PRO, PANalytical, Almelo, the Netherlands) at a scanning rate of 0.02°s^{-1} in a 2θ range of 10°–50°. The ratio of cubic/triclinic phase of Li_4WO_5-*x*LiF was calculated by the original XRD data. And the ratio of the main peak of cubic phase and triclinic phase represents the ratio of cubic and triclinic phase, respectively. The phase composition of the sintered ceramics was also confirmed by Raman spectrometer (DXR; Thermo Fisher Scientific, American). Selected area electron diffraction (SAED) data was performed with a JEM-2100 F at an accelerating voltage of 200 kV. The bulk densities were measured by Archimedes' method. To observe grain morphology, the polished and thermally etched surfaces of fired ceramics (fired 25 °C below the optimized sintering temperature) were observed with a Hitachi (Tokyo, Japan) S4800 field-emission scanning electron microscopy (FESEM). Meanwhile, the elemental mapping and energy-dispersive x-ray spectroscopy (EDS) were also measured by FESEM. The permittivity and the quality factor values were measured in the TE_{011} mode according to the Hakki-Coleman method using an Agilent N5230A network analyzer (Palo Alto, CA) in the temperature range of 25 °C–85 °C [20]. The temperature coefficient of the resonant frequency τ_f was calculated by Equation (1):

$$\tau_f = \frac{\Delta f}{f_1(T_2 - T_1)} \quad (1)$$

where $\Delta f = f_2 - f_1$, f_2 and f_1 were the resonant frequencies at the temperature of T_2 (85 °C) and T_1 (25 °C), respectively. The linear coefficient of thermal expansion (CTE) of the Li_4WO_5 and $Li_{3.1}W_{0.7}F_{0.3}O_{3.5}$ ceramics were estimated utilizing a thermal dilatometer (DIL402C, NETZSCH, Germany). The infrared spectra at room temperature were measured by a Bruker IFS 66v FT-IR spectrometer on the infrared beamline station (U4) at the National Synchrotron Radiation Lab (NSRL), China.

3. Result and discussions

Fig. 1(a–e) shows the room-temperature XRD patterns of the (1-*x*)Li_4WO_5-*x*LiF ((a) x = 0.1, (b) x = 0.2, (c) x = 0.3, (d) x = 0.4, (e) x = 0.5) ceramics sintered from 810 °C to 990 °C for 4 h. According to the previous reports, the Li_4WO_5 exhibited an irreversible phase transition from cubic to triclinic around 700 °C [8]. In the present work, this phase transformation was also observed. And the temperature of phase transformation changed with the x value in Fig. 1. Both the cubic Li_4WO_5 (JCPDS card No. 00-021-0531) and triclinic Li_4WO_5 (JCPDS card No. 01-088-0756) phase coexisted with the cubic phase prominent when samples sintered at low temperature, eg. 850 °C. With the increase of sintering temperature, the fraction

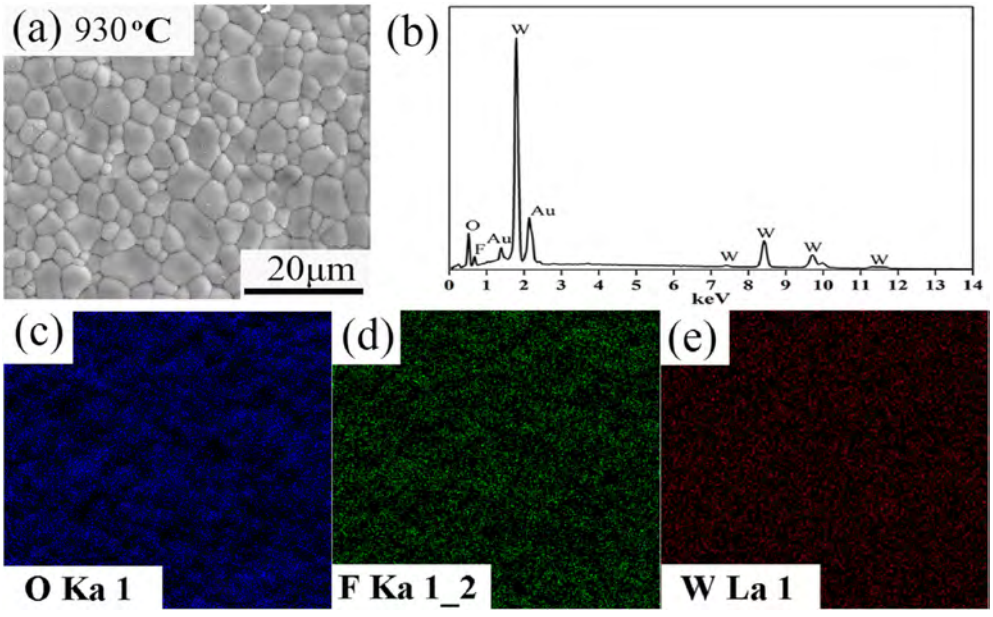

Fig. 3. SEM image (a), EDS spectrum (b) and EDS elemental mapping images (c) (d) (e) of the surface of $Li_{3.1}W_{0.7}F_{0.3}O_{3.5}$ ceramic sintered at 930 °C for 4 h.

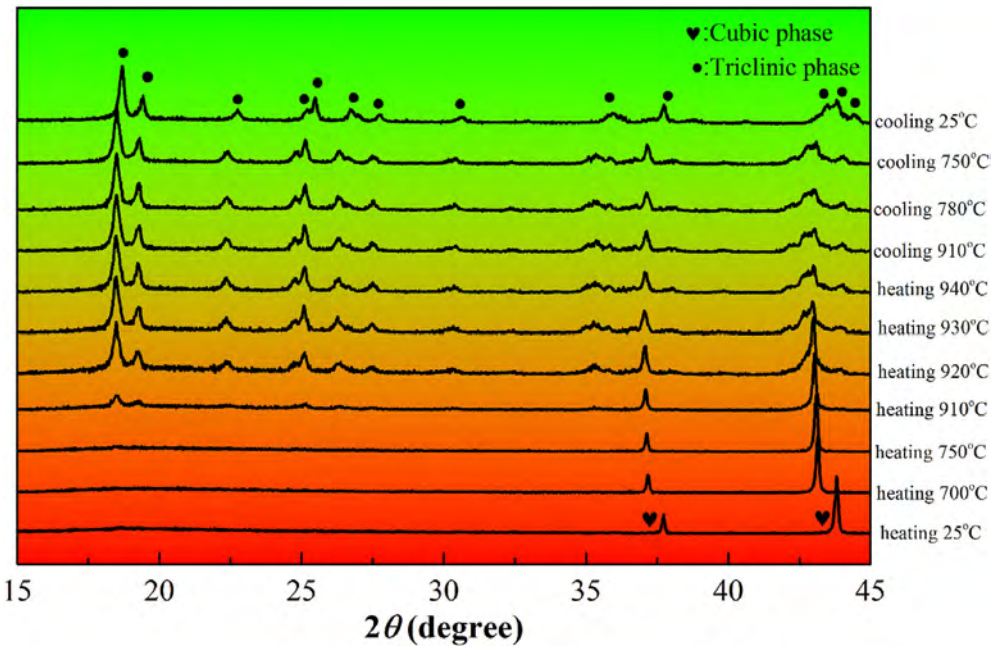

Fig. 4. The various-temperature XRD analysis was conducted on the $Li_{3.1}W_{0.7}F_{0.3}O_{3.5}$ ceramics sintered from room temperature to 950 °C.

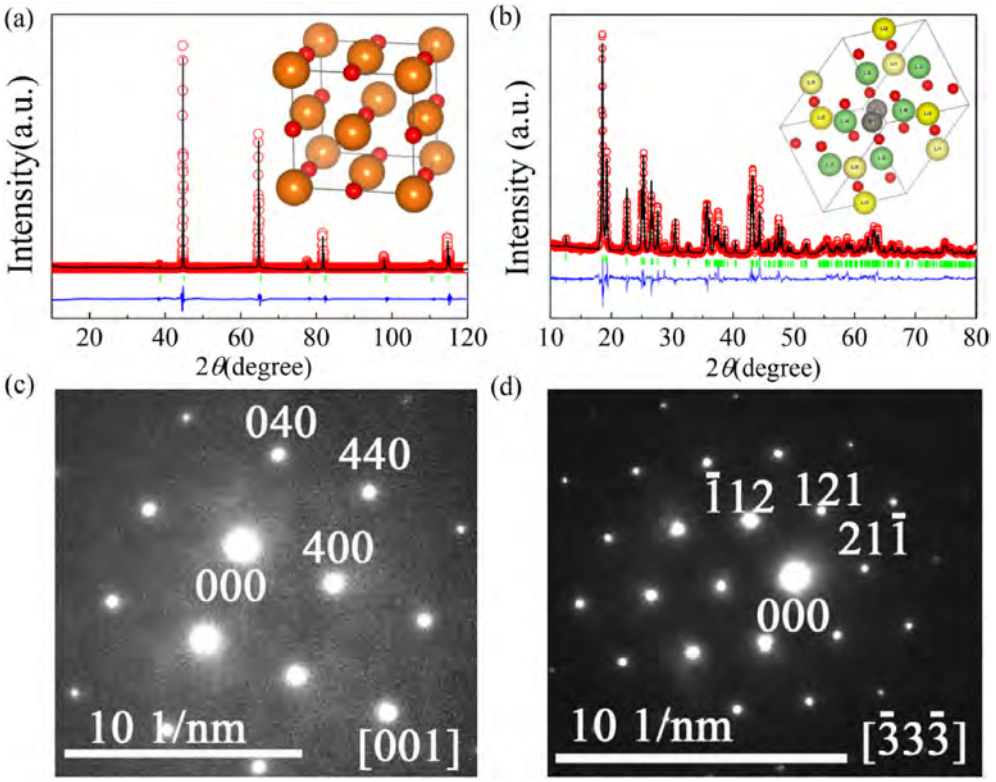

Fig. 5. (a) and (b) Rietveld refinement patterns and schematics of crystal structure for the cubic phase and triclinic phase of $Li_{3.1}W_{0.7}F_{0.3}O_{3.5}$, respectively; (c) and (d) selected area electron diffraction (SAED) images for the cubic phase and triclinic phase of $Li_{3.1}W_{0.7}F_{0.3}O_{3.5}$, respectively.

of the cubic phase gradually decreased. The cubic phase could fully transform to the triclinic phase ultimately at a critical temperature which depended on the LiF content. Fig. S1 shows the evolution in the ratio of cubic/triclinic phases (the dashed lines for the triclinic γ phase, and the solid lines for the cubic α phase) with respect to x value. The DTA curves show the phase transformation temperature increases with the increase of LiF content in Fig. 2, such as 700 °C for un-doped sample, 870 °C for $Li_{3.7}W_{0.9}F_{0.1}O_{4.5}$ ($x = 0.1$) ceramics and 970 °C for $Li_{2.5}W_{0.5}F_{0.5}O_{2.5}$ ($x = 0.5$) ceramics.

In the present system, two possible accommodation mechanisms of addition of LiF in the ceramic matrix are considered: (1) LiF might aggregate around the grain boundaries and facilitate

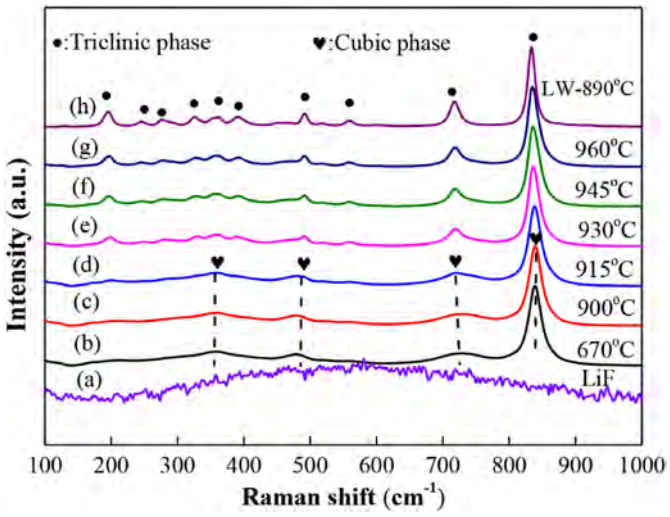

Fig. 6. The Raman spectra of LiF, $Li_{3.1}W_{0.7}F_{0.3}O_{3.5}$ sintered from 670 °C to 960 °C and pure Li_4WO_5 sintered at 890 °C, respectively.

densification through accelerating mass transfer process as sintering aids [16,17]. (2) LiF incorporated into the crystal lattice of Li_4WO_5 to form solid solutions; or both. In the view of compositional dependence of phase transformation temperature, LiF enters into Li_4WO_5 inducing evident effects on the degree of order of crystal structure. Based on the empirical Vegard's law, the lattice parameter of a solid solution is approximately linearly related to the molar fraction. Fig. 1(f) presents the variation in cell parameters of the triclinic phase as a function of LiF content. A nearly linear change is observed, providing direct evidence to verify the fact that LiF enters into the lattice of Li_4WO_5. The declining trend is attributed to the smaller ionic radius of F^- (1.19 Å) with respect to O^{2-} (1.26 Å). The SEM image of $Li_{3.1}W_{0.7}F_{0.3}O_{3.5}$ ceramics sintered at 930 °C shows a homogeneous and dense grain distribution (Fig. 3(a)). The element mapping analysis of $Li_{3.1}W_{0.7}F_{0.3}O_{3.5}$ ceramics is displayed in Fig. 3(c)–(e). The F element was distributed homogeneously in the entire region, and no element enrichment was observed at the grain boundary, indicating that LiF diffused into the lattice of Li_4WO_5. The results were consistent with those of the XRD and verified the solid solution formation.

In order to deeply understand the influence of LiF doping on phase transition of Li_4WO_5, various-temperature XRD analysis was conducted on $Li_{3.1}W_{0.7}F_{0.3}O_{3.5}$ over 25–950 °C (Fig. 4). Similarly, when measured at low temperature (<750 °C), only the cubic

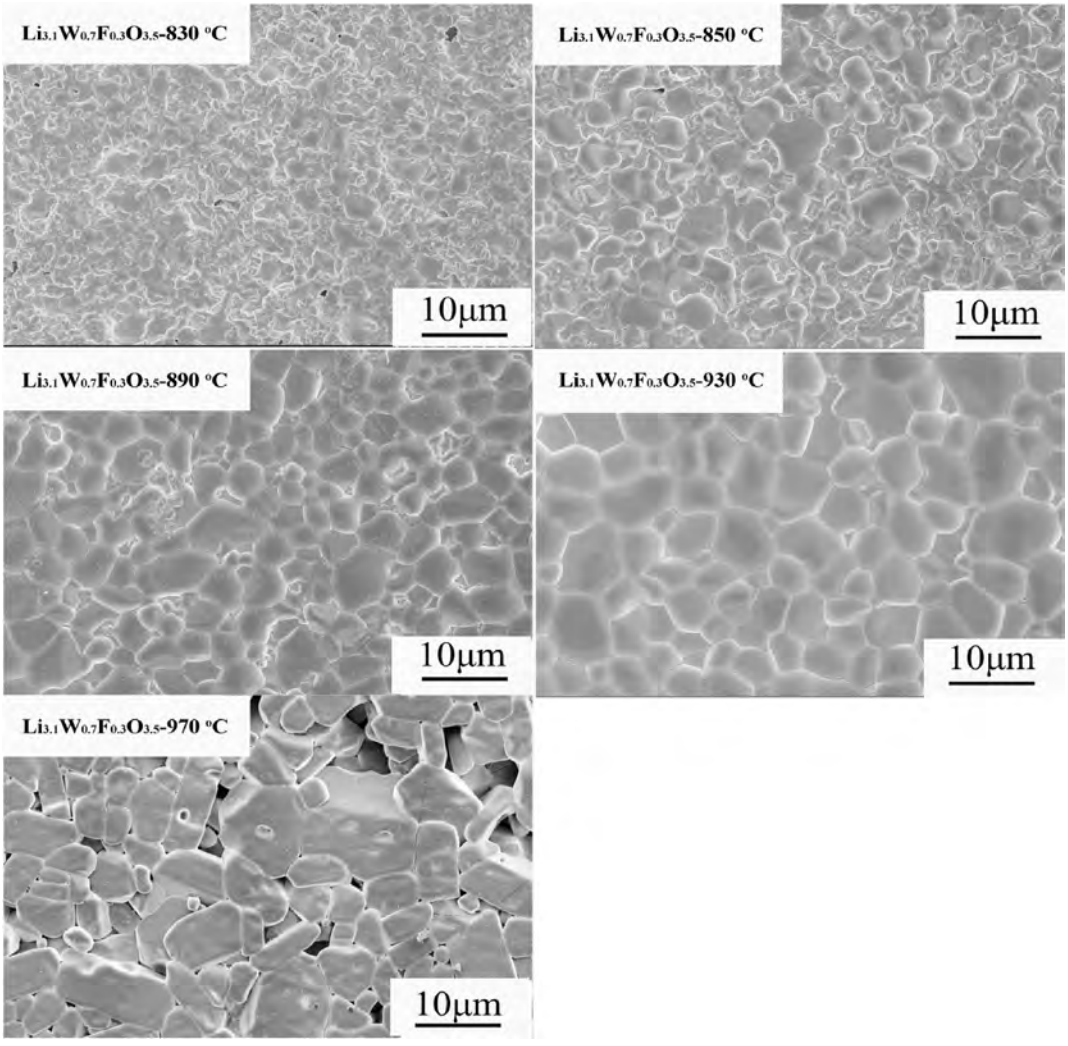

Fig. 7. The SEM images of $Li_{3.1}W_{0.7}F_{0.3}O_{3.5}$ ceramics sintered at different temperatures.

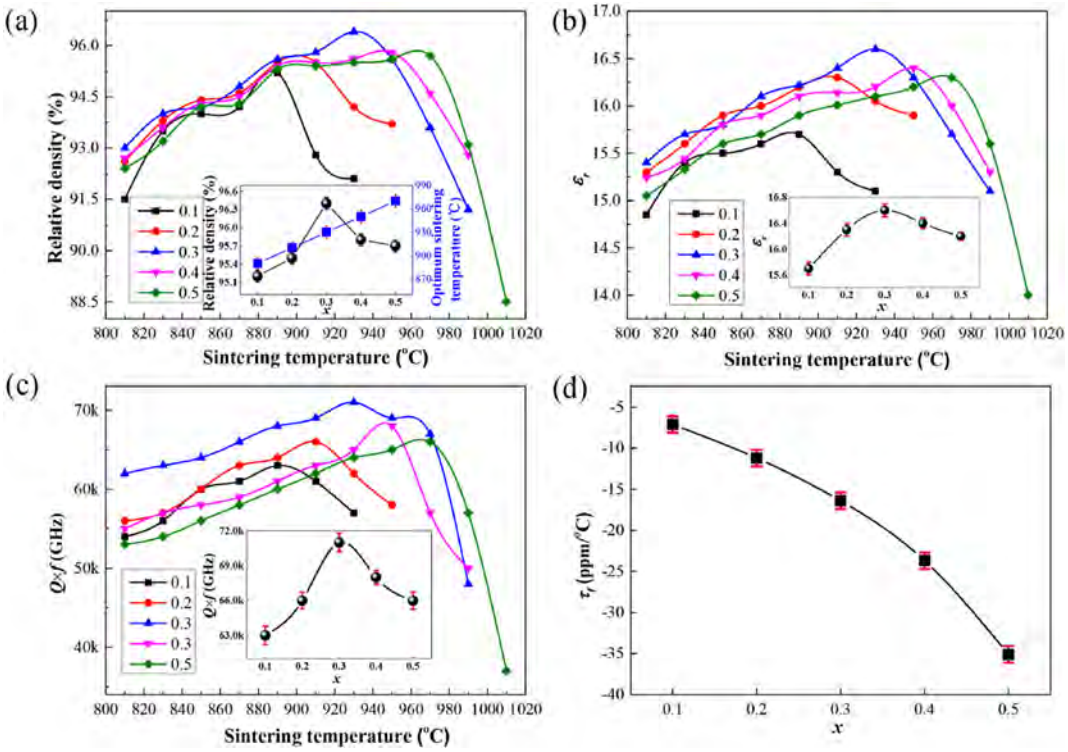

Fig. 8. The variations of the relative densities and microwave dielectric properties (ε_r, $Q \times f$, and τ_f) of (1-x)Li_4WO_5-xLiF (x = 0.1, 0.2, 0.3, 0.4, 0.5) ceramics sintered at different temperatures. And the illustration of Fig. 8(a–c) gives the best performance as a function of LiF concentration.

Table 1
Comparison of microwave dielectric properties of some compounds with rock salt structure sintered at the densification temperature.

Composition	S.T. (°C)	ε_r	$Q \times f$ (GHz)	τ_f (ppm/°C)	References
Li_4WO_5	890	8.6	23100	−2.6	[8]
Li_3NbO_4	1150	16.4	47100	−45	[17]
$0.3Li_3NbO_4 + 0.7Li_2SnO_3$	1200	13.5	61600	29	[28]
$Li_2ZrO_3 + 4MgO$	1500	12.65	165924	−34.66	[29]
$Li_2TiO_3 + 4MgO$	1600	13.43	233600	−27.2	[4]
$0.7Li_4WO_5 - 0.3LiF$	930	16.6	71000	−16.4	This work

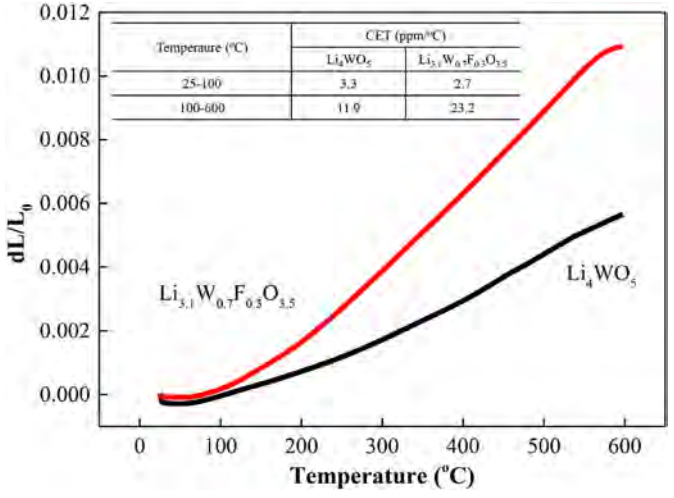

Fig. 9. The dilatometric curves of Li_4WO_5 and $Li_{3.1}W_{0.7}F_{0.3}O_{3.5}$ sintered at 890 °C and 930 °C.

Li_4WO_5 phase was detected while the triclinic Li_4WO_5 emerged at 800 °C and became dominated at 920 °C, finally a single triclinic Li_4WO_5 phase was obtained at 930 °C. When cooling down from elevated temperatures, the triclinic phase was stabilized up to room temperature, which was consistent with the irreversible feather of the phase transition. Additionally, obvious low-angle shift in XRD peaks was observed during heating process, while high-angle shift when cooling down, suggesting Li_4WO_5-based ceramics are materials with positive thermal expansion. Meanwhile, Fig. 5(a) and (b) show Rietveld refinement patterns and schematics of crystal structure for the cubic and triclinic phase of $Li_{3.1}W_{0.7}F_{0.3}O_{3.5}$, respectively. Structural models with a space group Fm-3m and P-1 were used for refinement, respectively. The results of the Rietveld refinement using the powder XRD data are listed in Table S1 (Supplementary information). Fig. 5(c) shows the cubic phase of $Li_{3.1}W_{0.7}F_{0.3}O_{3.5}$ from the selected area electron diffraction (SAED) images. The distances of the diffraction spots measured are 2.06 Å and 1.45 Å corresponding to d_{400} and d_{440} spacing, respectively. Fig. 5(d) shows the triclinic phase of $Li_{3.1}W_{0.7}F_{0.3}O_{3.5}$, the distances of the diffraction spots are 2.20 Å and 2.19 Å corresponding to $d\bar{1}12$ and $d21\bar{1}$ spacing, respectively.

In order to determine whether LiF existed and the phase transition process of $Li_{3.1}W_{0.7}F_{0.3}O_{3.5}$ occurred. Raman spectra was conducted on $Li_{3.1}W_{0.7}F_{0.3}O_{3.5}$ ceramic, as shown in Fig. 6. The

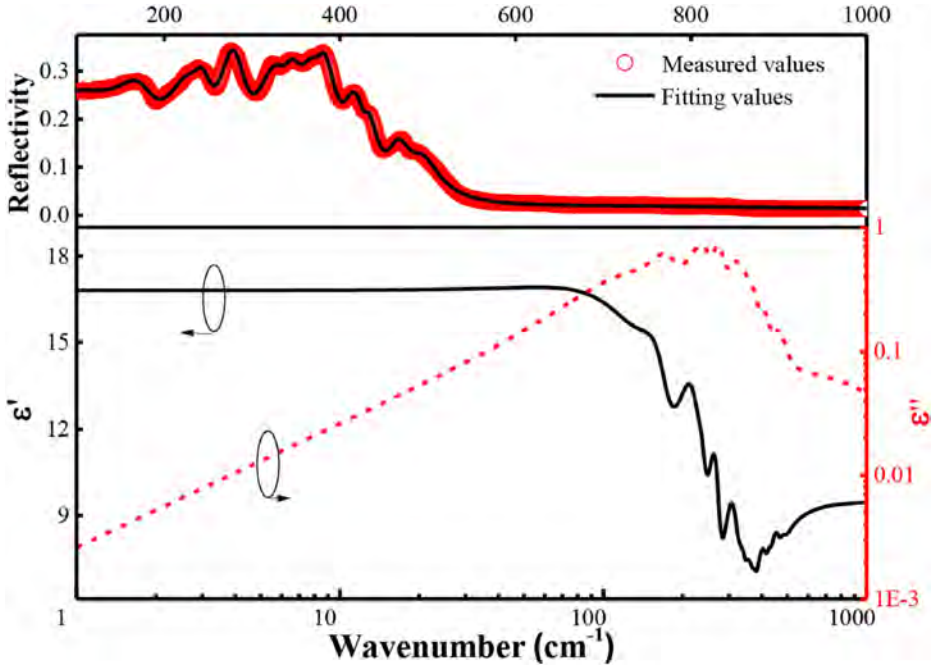

Fig. 10. The infrared reflectivity spectra of the $Li_{3.1}W_{0.7}F_{0.3}O_{3.5}$ ceramics in the range 100 cm^{-1}–1000 cm^{-1}.

phase transition temperature from cubic (the stretch mode marked as peach shape) to the triclinic (the stretch mode marked as circular point) phase is between 915 °C and 930 °C. No Raman mode of LiF exits in the temperature range of 670 °C–960 °C. At the same time, $Li_{3.1}W_{0.7}F_{0.3}O_{3.5}$ phase transition occurs with the increase of sintering temperature. The half-peak width of the whole stretching vibration peak of Raman becomes narrower, which indicates that the order degree of high temperature phase is higher than that of low temperature phase [21]. The effect of LiF content on the transformation temperature of (1-x)Li_4WO_5-xLiF (x = 0.1, 0.2, 0.4, 0.6, 1.0) is explained as follow. As the content of LiF increases, the order degree of oxyfluorides decreases and the transformation from cubic to triclinic phase is inhibited. Hence, higher temperature is needed to enhance the order degree up to critical point and then phase transition could occur. The similar phenomenon of rock salt Li_2TiO_3–MgO ceramics has been reported [19], with the decrease of order degree by forming solid solutions. The difference is that the phase transition of Li_2TiO_3–MgO binary system is from monoclinic to cubic phase. Therefore, the temperature of the order-disorder phase transition falls rapidly with the increase of MgO content.

Fig. 7 gives the SEM images of the $Li_{3.1}W_{0.7}F_{0.3}O_{3.5}$ ceramics sintered at different temperatures. Microstructural evolution is clearly distinguished with obvious grain growth with the increase of sintering temperature. Particularly, compared with the nominal Li_4WO_5 composition, the microstructure of LiF-doped samples was significantly improved. Dense microstructures with well-developed grains and distinct grain boundaries were achieved. The dynamic mechanism of densification improvement is unclear yet, but it is expected that the low melting point of LiF is partially responsible.

Fig. 8 shows the variations in the relative densities and microwave dielectric properties (ε_r, $Q \times f$, and τ_f) of (1-x)Li_4WO_5-xLiF (x = 0.1, 0.2, 0.3, 0.4, 0.5) ceramics sintered at different temperatures. The relative densities of all the compositions exhibit substantial dependence on sintering temperature. It shows a steady increase followed by a dramatic drop after approaching the highest density. Importantly, all the samples achieved relative densities higher than 95% at their respective optimum sintering temperatures.

The variation trend of the ε_r and $Q \times f$ with sintering temperature is consistent with the density, proving that density exert prominent influences on the microwave dielectric properties (Fig. 8(b) and (c)). The compositional dependences of ε_r and $Q \times f$ values are presented in the inset of Fig. 8(b) and (c). When x = 0.3, the optimum microwave dielectric performances with ε_r = 16.6, and $Q \times f$ = 71,000 GHz were obtained. The permittivity at microwave frequencies relies on the relative densities, secondary phases and ionic polarizability [22,23]. In our previous study, the theoretical relative permittivity value ~10.15 of Li_4WO_5 was calculated by Clausius-Mossotti equation [8]. Generally, the factors effecting the dielectric loss could be divided into two major components: the intrinsic loss and extrinsic loss relying on impurities, grain boundaries, density, lattice defects, etc [24]. In the present work, the high $Q \times f$ value usually corresponds to the high densification. Interestingly, the τ_f value steadily decreases with the increase of x content from −7.12 ppm/°C at x = 0.1 to −35.11 ppm/°C at x = 0.5, as shown in Fig. 7(d). This phenomenon may attribute to τ_f = -3 ppm/°C of pure Li_4WO_5 and τ_f = -120 ppm/°C of LiF. Hence, on the basis of the classical phase rule, τ_f decreases with the increase of LiF content [25].

The microwave dielectric properties of some compounds with rock salt structure are listed in Table 1. Compared with the pure Li_4WO_5, the $Q \times f$ value of $Li_{2.8}W_{0.6}F_{0.4}O_3$ dramatically increases due to the distinct improvement of density. Besides, $Li_{3.1}W_{0.7}F_{0.3}O_{3.5}$ has lower sintering temperature and better microwave dielectric properties in rock salt structure compounds. In summary, $Li_{3.1}W_{0.7}F_{0.3}O_{3.5}$ ceramic is a promising candidate in LTCC technology.

The dilatometric curves of Li_4WO_5 and $Li_{3.1}W_{0.7}F_{0.3}O_{3.5}$ ceramics are shown in Fig. 9. Compared with the nominal Li_4WO_5, $Li_{3.1}W_{0.7}F_{0.3}O_{3.5}$ ceramic has a larger coefficient of thermal expansion (CTE) from the dilatometric curves. At lower temperature range (20 °C–100 °C), relatively lower thermal expansion with a CTE around 3 ppm/°C were obtained, then increased to about

23 ppm/°C at elevated temperature up to 600 °C for $Li_{3.1}W_{0.7}F_{0.3}O_{3.5}$. This CTE value is close to that of Ag (19.5 ppm/°C), commonly used as electrode in LTCC technology, which is of significance to render good thermal expansion match between the ceramic matrix and Ag electrode in practical application [26].

Fig. 10 presents the infrared reflectivity spectra of the $Li_{3.1}W_{0.7}F_{0.3}O_{3.5}$ ceramics in the range of 100–1000 cm^{-1}. These spectra were analyzed and fitted using the classical harmonic oscillator model and the Fresnel formula [22,27]:

$$\varepsilon^*(\omega) = \varepsilon_\infty + \sum_{j=1}^{n} \frac{\omega_{pj}^2}{\omega_{oj}^2 - \omega^2 - ir_j\omega} \quad (2)$$

$$R(\omega) = \left|\frac{1 - \sqrt{\varepsilon^*(\omega)}}{1 + \sqrt{\varepsilon^*(\omega)}}\right|^2 \quad (3)$$

where $\varepsilon^*(\omega)$ is complex dielectric function, and ε_∞ is the dielectric constant at the high-frequency limit; ω_{oj}, r_j, and ω_{pj}, are the transverse frequency, damping factor and the plasma frequency of the j-th Lorentz oscillator, respectively; n and $R(\omega)$ are the number of transverse phonon modes and the IR reflectivity. The infrared spectra can be well fitted and phonon parameters are shown in Table S3 (Supplementary information). Moreover, the calculated permittivity ε' and the dielectric loss ε'' obtained from the fits of the infrared reflectivity. These values match well with those measured using TE_{011} method.

4. Conclusions

(1-x)Li_4WO_5-xLiF (x = 0.1, 0.2, 0.3, 0.4, 0.5) ceramics were prepared by conventional solid-state reaction method. A series of novel oxyfluorides in the Li_4WO_5–LiF binary system were prepared by adding an appropriate amount of LiF into Li_4WO_5. The temperature of phase transition (cubic-triclinic phase) moved towards high temperature with the increase of LiF content. $Li_{3.1}W_{0.7}F_{0.3}O_{3.5}$ ceramics (96.4%) sintered at 930 °C for 4 h could be obtained with excellent microwave dielectric properties ($Q \times f$ = 71,000 GHz, ε_r = 16.6, τ_f = −16.4 ppm/°C). The infrared reflectivity spectra of the $Li_{3.1}W_{0.7}F_{0.3}O_{3.5}$ ceramics revealed that the quality factor of Li_4WO_5 was drastically improved by doping LiF. Therefore, the Li_4WO_5–LiF binary system was a promising candidate for microwave electronic device applications.

Declaration of competing interest

The authors declare that they have no known competing financial interests or personal relationships that could have appeared to influence the work reported in this paper.

CRediT authorship contribution statement

Kai Xiao: Data curation, Writing - original draft. **Chunchun Li:** Conceptualization, Methodology. **Ying Tang:** Supervision, Formal analysis, Writing - review & editing. **Yunfei Tian:** Data curation. **Changzhi Yin:** Data curation. **Junqi Chen:** Data curation. **Jie Li:** Formal analysis, Writing - review & editing. **Lian Duan:** Data curation. **Huaicheng Xiang:** Data curation. **Liang Fang:** Resources, Supervision, Funding acquisition.

Acknowledgments

This work was financially supported by the Natural Science Foundation of China (Nos. 21761008 and 21965009), the Natural Science Foundation of Guangxi Zhuang Autonomous Region (Nos. 2018GXNSFAA138175, and 2018GXNSFBA281093), the Project of Scientific Research and Technical Exploitation Program of the Guangxi Zhuang Autonomous Region (No. AA18118008, AA18118034 and AA18118023), and Projects of Education Department of Guangxi Zhuang Autonomous Region (No. 2018KY0255) and High level innovation team and outstanding scholar program of Guangxi Institutes. The author thanks the administrator of the IR beamline workstation at the National Synchrotron Radiation Laboratory (NSRL) for their assistance in IR measurements and Dr. Hongbo Cui of the Guilin University of Technology for his help with the TEM measurements.

Appendix A. Supplementary data

Supplementary data to this article can be found online at https://doi.org/10.1016/j.jallcom.2020.155320.

References

[1] C. Tseng, P. Tseng, C. Chang, Y. Kao, Novel temperature stable Li_2MnO_3 microwave dielectric ceramics with high Q for LTCC applications, J. Am. Ceram. Soc. 97 (2014) 1918–1922.
[2] J.J. Bian, Y.F. Dong, New high Q microwave dielectric ceramics with rock salt structures: $(1-x)Li_2TiO_3 + xMgO$ system ($0 \le x \le 0.5$), J. Eur. Ceram. Soc. 30 (2010) 325–330.
[3] Y.W. Tseng, J.Y. Chen, Y.C. Kuo, C.L. Huang, Low-loss microwave dielectrics using rock salt oxide Li_2MgTiO_4, J. Alloys Compd. 509 (2011) L308–L310.
[4] J.X. Bi, C.C. Li, Y.H. Zhang, C.F. Xing, C.H. Yang, H.T. Wu, Crystal structure, infrared spectra and microwave dielectric properties of ultra low-loss $Li_2Mg_4TiO_7$ ceramics, Mater. Lett. 196 (2017) 128–131.
[5] Z. Fu, P. Liu, J. Ma, X. Zhao, H. Zhang, Novel series of ultra-low loss microwave dielectric ceramics: $Li_2Mg_3BO_6$ (B = Ti, Sn, Zr), J. Eur. Ceram. Soc. 36 (2016) 625–629.
[6] J. Bi, Y. Niu, H. Wu, $Li_4Mg_3Ti_2O_9$: a novel low-loss microwave dielectric ceramic for LTCC applications, Ceram. Int. 43 (2017) 7522–7530.
[7] H.L. Pan, H.T. Wu, Crystal structure, infrared spectra and microwave dielectric properties of new ultra low-loss $Li_6Mg_7Ti_3O_{16}$ ceramics, Ceram. Int. 43 (2017) 14484–14487.
[8] J. Li, L. Fang, H. Luo, J. Khaliq, Y. Tang, C.C. Li, Li_4WO_5: a temperature stable low-firing microwave dielectric ceramic with rock salt structure, J. Eur. Ceram. Soc. 36 (2016) 243–246.
[9] R.J. Cava, Dielectric materials for applications in microwave communications, J. Mater. Chem. 11 (2001) 54–62.
[10] T.A. Vanderah, Talking ceramics, Science 298 (2002) 1182–1184.
[11] M.T. Sebastian, R. Ubic, H. Jantunen, Low-loss dielectric ceramic materials and their properties, Int. Mater. Rev. 60 (2015) 392–412.
[12] K. Xiao, C.C. Li, H.C. Xiang, L. Fang, Reaction sintering of a rock salt structured Li_4WO_5 ceramic and its microwave dielectric properties, J. Mater. Sci. Mater. Electron. 29 (2018) 6397–6402.
[13] C.C. Li, H. Luo, H.C. Xiang, Y. Tang, L. Fang, Sintering behavior, microstructure, and microwave dielectric properties of $Li_{4(1+x)}WO_5$ ($0 \le x \le 0.08$), J. Electron. Mater. 46 (2017) 4047–4051.
[14] L.X. Pang, D. Zhou, Microwave dielectric properties of low-firing Li_2MO_3 (M = Ti, Zr, Sn) ceramics with B_2O_3-CuO addition, J. Am. Ceram. Soc. 93 (2010) 3614–3617.
[15] Z. Wang, B. Huang, L. Wang, Z. Fu, Q. Zhang, Sintering characteristics and microwave dielectric properties of $Ba(Co_{1/3}Nb_{2/3})O_3$–MnO_2 ceramics, J. Mater. Sci. Mater. Electron. 26 (2015) 1107–1112.
[16] Z.F. Fu, J.L. Ma, P. Liu, B.C. Guo, X.M. Chen, Microwave dielectric properties of low-fired Li_2MnO_3 ceramics co-doped with LiF-TiO_2, Ceram. Int. 42 (2016) 6005–6009.
[17] J.J. Bian, J.Y. Wu, L. Wang, Structural evolution, sintering behavior and microwave dielectric properties of (1 − x) Li3NbO4 − xLiF ($0 \le x \le 0.9$), J. Eur. Ceram. Soc. 32 (2012) 1251–1259.
[18] Y.Z. Hao, H. Yang, G.H. Chen, Q.L. Zhang, Microwave dielectric properties of Li_2TiO_3 ceramics doped with LiF for LTCC applications, J. Alloys Compd. 552 (2013) 173–179.
[19] M. Castellanos, A.R. West, Order-disorder phenomena in oxides with rock salt structures: the system Li_2TiO_3-MgO, J. Mater. Sci. 14 (1979) 450–454.
[20] B.W. Hakki, P.D. Coleman, Method of measuring inductive capacities in the millimeter range, IRE Trans. Microw. *Theory Tech., MTT-* 8 (1960) 402–410.
[21] S.-K. Singh, S.-R. Kiran, V.R.K. Murthy, Raman spectroscopic and microwave dielectric studies on spinel $Li_2Zn_{(1-x)}Ni_xTi_3O_8$, compounds, Mater. Chem. Phys. 141 (2013) 822–827.
[22] C.C. Li, H.C. Xiang, M.Y. Xu, J. Khaliq, J.Q. Chen, L. Fang, Low-firing and temperature stable microwave dielectric ceramics: $Ba_2LnV_3O_{11}$ (Ln=Nd, Sm), J. Am. Ceram. Soc. 101 (2018) 773–781.
[23] C.C. Li, H.C. Xiang, M.Y. Xu, Y. Tang, L. Fang, Li_2AGeO_4 (A= Zn, Mg): two novel

low-permittivity microwave dielectric ceramics with olivine structure, J. Eur. Ceram. Soc. 38 (2018) 1524–1528.
[24] C.C. Li, C.Z. Yin, J.Q. Chen, H.C. Xiang, Y. Tang, L. Fang, Crystal structure and dielectric properties of germanate melilites $Ba_2MGe_2O_7$ (M= Mg and Zn) with low permittivity, J. Eur. Ceram. Soc. 38 (2018) 5246–5251.
[25] X.Q. Song, K. Du, J. Li, X.K. Lan, W.Z. Lu, X.H. Wang, W. Lei, Low-fired fluoride microwave dielectric ceramics with low dielectric loss, Ceram. Int. 45 (2019) 279–286.
[26] U. Santhosh, J. Ahmad, A model for estimating nonlinear deformation and damage in ceramic matrix composites, J. Compos. Mater. 47 (2013) 1257–1272.
[27] J. Guo, D. Zhou, L. Wang, H. Wang, T. Shao, Z.M. Qi, X. Yao, Infrared spectra, Raman spectra, microwave dielectric properties and simulation for effective permittivity of temperature stable ceramics $AMoO_4$-TiO_2 (A = Ca, Sr), Dalton T 42 (2013) 1483–1491.
[28] N.X. Wu, J.J. Bian, Microstructure and microwave dielectric properties of $(1-y)Li_3NbO_4 + yLi_2TiO_3$ (Li_2SnO_3) ceramics, Mater. Sci. Eng., B 177 (2012) 1793–1798.
[29] J.X. Bi, C.F. Xing, C.H. Yang, H.T. Wu, Phase composition, microstructure and microwave dielectric properties of rock salt structured Li_2ZrO_3-MgO ceramics, J. Eur. Ceram. Soc. 38 (2018) 3840–3846.